Eur. Phys. J. D **54**, 153–158 (2009)
DOI: 10.1140/epjd/e2009-00040-x

THE EUROPEAN PHYSICAL JOURNAL D

Regular Article

Electrohydrodynamic flow in a wire-plate non-thermal plasma reactor measured by 3D PIV method

J. Podlinski[1,a], A. Niewulis[1], and J. Mizeraczyk[1,2]

[1] Centre for Plasma and Laser Engineering, The Szewalski Institute of Fluid Flow Machinery, Polish Academy of Sciences, Fiszera 14, 80-952 Gdańsk, Poland
[2] Department of Marine Electronics, Gdynia Maritime University, Morska 81-87, 81-225 Gdynia, Poland

Received 3rd September 2008 / Received in final form 21st December 2008
Published online 13 February 2009 – © EDP Sciences, Società Italiana di Fisica, Springer-Verlag 2009

Abstract. This work was aimed at measurements of the electrohydrodynamic (EHD) secondary flow in a non-thermal plasma reactor using three-dimensional particle image velocimetry (3D PIV) method. The wide-type non-thermal plasma reactor used in this work was an acrylic box with a wire discharge electrode and two plate collecting electrodes. The positive DC voltage was applied to the wire electrode through a 10 MΩ resistor. The collecting electrodes were grounded. The voltage applied to the wire electrode was 28 kV. Air flow seeded with a cigarette smoke was blown along the reactor duct with an average velocity of 0.6 m/s. The 3D PIV velocity fields measurements were carried out in four parallel planes stretched along the reactor duct, perpendicularly to the wire electrode and plate electrodes. The measured flow velocity fields illustrate complex nature of the EHD induced secondary flow in the non-thermal plasma reactor.

PACS. 47.65.-d Magnetohydrodynamics and electrohydrodynamics – 52.30.-q Plasma dynamics and flow – 52.25.Fi Transport properties

1 Introduction

Non-thermal plasma techniques have become an important tool for controlling the emission of various gaseous pollutants, such as acid gases (SO_x, NO_x, HCl, etc.), greenhouse gases (CO_x, N_xO_y, perfluorocompounds, etc.), ozone depletion gases (freons, halons, etc.), volatile organic compounds (VOCs, e.g. toluene, xylene, etc.) and toxic gases (Hg, dioxins, etc.). The main advantages of the non-thermal plasma techniques are small space volume, low cost, high pollutant removal and energy efficiencies.

Ohkubo et al. [1] and Kanazawa et al. [2] found that the removal of NO molecules in a needle-to-plate and corona discharge radical shower (CDRS) non-thermal plasma reactors occurred not only in the streamer corona discharge and downstream regions of the reactors but also in the reactor upstream region. The reason of the NO removal in the upstream region of the reactor was not clear. However, the results of the electrohydrodynamic (EHD) secondary flow (ionic wind) measurements in non-thermal plasma reactors [3–6] suggest that the EHD flow is capable of transporting long-living active species, such as ozone, upstream of the discharge region, where they may react with other species. Hence, if the ozone molecules were transported by the EHD flow upstream of the discharge region in the experiment of Ohkubo et al. [1] and Kanazawa et al. [2], they would be long-live and active enough to oxidize NO molecules and efficiently remove them before they reach the discharge region. Results presented in [1–6] show great importance of the EHD secondary flow on non-thermal plasma reactors operation. Collecting data about flow in non-thermal plasma reactors is important for designing reactors of high performance efficiency. Therefore, there are many numerical works for EHD flow [7–9].

This work was aimed at measurements of the EHD flow in a wire-plate non-thermal plasma reactor. Since our previous results [3–6] only suggested 3-dimensional nature of the EHD secondary flow we measured all three flow components using three-dimensional particle image velocimetry (3D PIV) method [10]. Our measurements were carried out in four parallel planes and showed complex 3D nature of the EHD induced secondary flow and a great importance of the side wall effects.

2 Experimental set-up

The apparatus used in this experiment consisted of a wide-type non-thermal plasma reactor, DC high voltage supply and a standard 3D particle image velocimetry (PIV) equipment for the flow velocity field measurement (Fig. 1).

[a] e-mail: janusz@imp.gda.pl

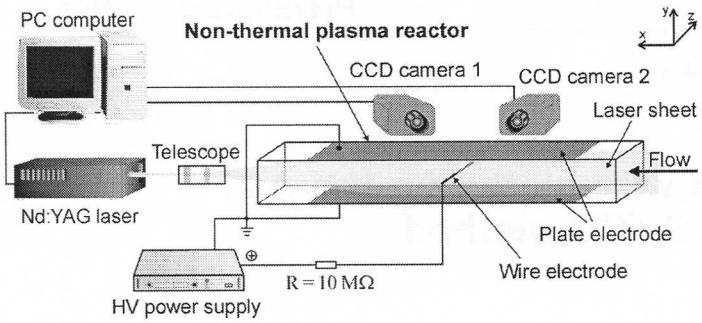

Fig. 1. Experimental set-up for 3D-PIV flow velocity field measurements in non-thermal plasma reactor.

The wide-type non-thermal plasma reactor used in this work was an acrylic box 1000 mm long, 200 mm wide and 100 mm high. The electrical electrode set consisted of a wire discharge electrode and two plate electrodes. The wire electrode (diameter 1 mm, length 200 mm) was placed perpendicularly to the main flow, in the middle of the non-thermal plasma reactor between the plate electrodes, which were placed on the top and bottom of the reactor. The width of each plate electrodes was 200 mm, while the plate-to-plate electrode spacing was 100 mm. A flow homogenizer was placed before the reactor inlet.

Air flow seeded with a cigarette smoke (majority of smoke particles with diameter lower than 1 μm in dry air) was blown along the reactor duct with an average velocity of 0.6 m/s. The positive DC voltage of 28 kV was applied to the wire electrode through a 10 MΩ resistor, while the plate electrodes were grounded. The averaged discharge current was 130 μA. For such parameter corona discharge occurred in the non-thermal plasma reactor.

The standard 3D PIV equipment consisted of a twin second harmonic Nd-YAG laser system (λ = 532 nm), imaging optics (cylindrical telescope), two CCD cameras and a PC computer with Dantec FlowManager software.

To measure three components of velocity vector two CCD cameras have to observe the same measurement area under different angles. Determining real value of particle velocity vector one should make sure that both cameras observe the same area. Therefore a calibration procedure should be carried out. It entails placing a calibration target in the place of laser sheet. Calibration target contains markers which allow to define zero point (point, where $x = 0$ and $y = 0$), direction of X and Y axis as well as a numerical representation of the measurement area on the CCD element of both cameras. Upon carrying out calculation of an image of two cameras it was possible to obtain two two-dimensional (2D) vector maps of flow velocity fields. Then, using these two 2D vector maps and data obtained in calibration procedure it is possible to calculate one three-dimensional (3D) velocity vector map.

The 3D PIV measurements were carried out in four parallel planes (A, B, C and D) placed perpendicularly to both electrodes. The plane A was placed in the reactor midplane i.e. 100 mm from the side walls, when the planes B, C and D were placed 60 mm, 20 mm and 10 mm from the side wall, respectively (Fig. 2).

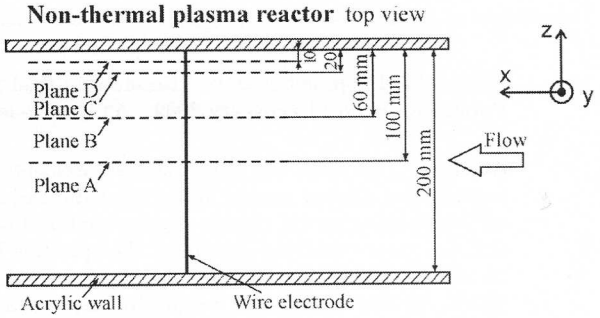

Fig. 2. Non-thermal plasma reactor top view. Measurement planes A, B, C and D marked by dashed lines.

For each measurement plane flow measurements were carried out in two overlapping observation areas. The first observation area (the area of the laser sheet "seen" by both CCD cameras) covered a region between the plate electrodes, ranging from $x = -200$ mm to $x = 20$ mm. The second observation area covered a region between the plate electrodes, ranging from $x = -20$ mm to $x = 200$ mm. Hence, the total observation area ranging from $x = -200$ mm to $x = 200$ mm.

Flow velocity fields presented in this paper resulted from averaging of 100 3D PIV instantaneous results, which means that presented flow velocity fields are time-averaged. These flow velocity fields are presented in this paper as vector maps and gray scale maps. The vector maps show flow velocity fields in the measurement plane i.e. velocity x- and y-component, while the gray scale maps show velocity z-component (perpendicular to the measurement plane). Based on the averaged velocity fields the flow streamlines were calculated.

3 Results

When no voltage was applied the measured flow in the non-thermal plasma reactor was laminar (results not presented in this paper). After applying a high voltage to the wire electrode, the electric forces exerted by the electric field on the space charge generated by corona discharge induced a noticeable EHD secondary flow of the gas which altered drastically the primary laminar flow. Besides, the electric force exerted on each individual dust particle with

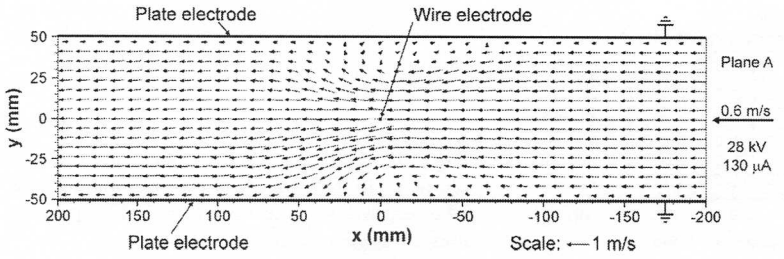

Fig. 3. Averaged flow velocity field in the plane A in the non-thermal plasma reactor. The applied voltage was 28 kV. The primary flow average velocity was 0.6 m/s.

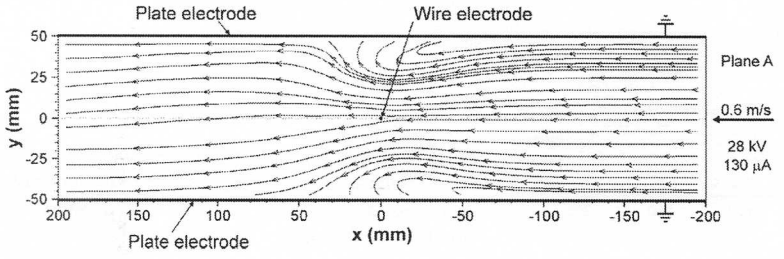

Fig. 4. Flow streamlines in the plane A in the non-thermal plasma reactor. The applied voltage was 28 kV. The primary flow average velocity was 0.6 m/s.

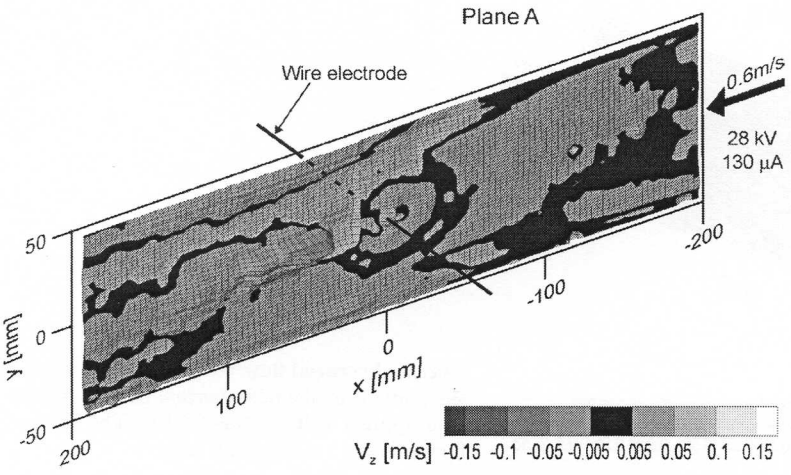

Fig. 5. Averaged flow velocity z-component in the plane A in the non-thermal plasma reactor. The applied voltage was 28 kV. The primary flow average velocity: 0.6 m/s.

charge q_p induces a drift of the particle with respect to the suspending air. Therefore, the net motion of the charged dust particles has two components, one due to the gas flow and the other, the particle drift velocity, due to the electric force $q_p\boldsymbol{E}$ (where $\boldsymbol{E}$ is the electric field). For submicron particles, except just around the wire electrode (where $\boldsymbol{E}$ is very strong), the particle drift velocity is much lower than the gas velocity [11]. Therefore, we can assume that, to a first approximation, the charged dust particles follow the gas flow. Hence, the particle flow velocity fields we measured represent also the gas flow velocity fields in the non-thermal plasma reactor, except just around the wire.

Figures 3–14 show results of the 3D PIV measurements in the non-thermal plasma reactor when the average primary flow velocity was 0.6 m/s and positive voltage of 28 kV was applied. The average total discharge current was 130 μA. At this conditions, the Reynolds number was $\mathrm{Re} = V \times L/\nu = 3820$ [12]. The parameters used to calculate Re were: the primary flow average velocity $V = 0.6$ m/s, the characteristic length (plate-plate distance) $L = 0.1$ m, and the air kinematic viscosity $\nu = 1.57 \times 10^{-5}$ m^2/s. The EHD number, which is related to the electric forces, was 5.5×10^7. The EHD number was calculated using a formula: $\mathrm{Ehd} = I \times L^3/(\nu^2 \times \rho \times \mu_i \times A)$ [12], with the parameters as follows: $I = 130$ μA (the average total discharge current), $L = 0.1$ m (the distance between the collecting electrodes), $\nu = 1.57 \times 10^{-5}$ m^2/s (the air kinematic viscosity), $\rho = 1.205$ kg/m^3 (the air density), $A = 0.1$ m $\times 0.2$ m $\times 2 = 0.04$ m^2 (the discharge area – the 100 mm-wide region along the wire electrode on both plate electrodes) and $\mu_i = 2 \times 10^{-4}$ m^2/V s (the ion mobility). The ratio of the EHD number to the Reynolds number squared ($\mathrm{Ehd}/\mathrm{Re}^2$ describes the ratio of the electric force to the inertial force) was 3.8, so the electric force dominate over the inertial one (for $\mathrm{Ehd}/\mathrm{Re}^2$ lower than 1 the inertial force will dominate over the electric force).

Figures 3–5 show the averaged flow patterns in the midplane (plane A) in the non-thermal plasma reactor. As

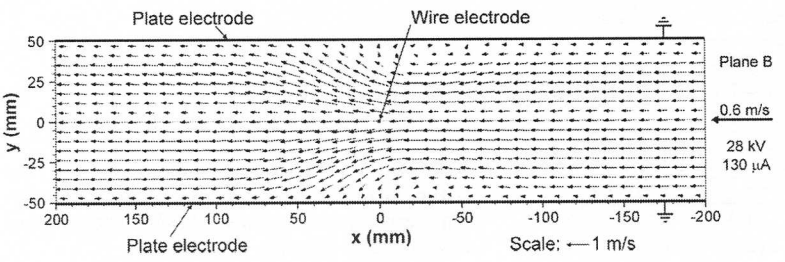

Fig. 6. Averaged flow velocity field in the plane B in the non-thermal plasma reactor. The applied voltage was 28 kV. The primary flow average velocity was 0.6 m/s.

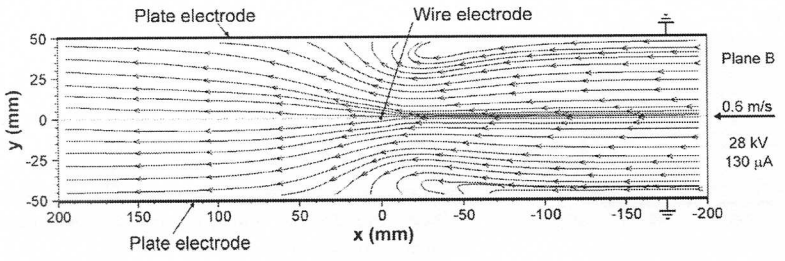

Fig. 7. Flow streamlines in the plane B in the non-thermal plasma reactor. The applied voltage was 28 kV. The primary flow average velocity was 0.6 m/s.

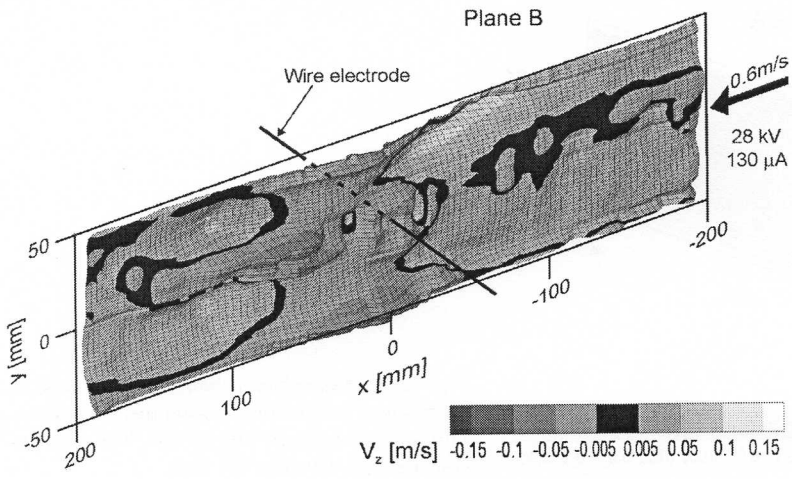

Fig. 8. Averaged flow velocity z-component in the plane B in the non-thermal plasma reactor. The applied voltage was 28 kV. The primary flow average velocity: 0.6 m/s.

can be seen, there are no significant flow disturbances in the upstream of the discharge region (for x from –200 mm to –50 mm). In the discharge region (x from –50 mm to 50 mm) the flow is blocked near the plate electrodes and flow rather by the central part of the channel, close to the discharge electrode. After passing the discharge electrode the flow spreads up to the plate electrodes. In the downstream of the discharge region (x from 50 mm to 200 mm) the flow pattern again became quite regular and directed in accordance with the primary flow direction. The flow velocity z-component in this plane (presented in Fig. 5) is very low (lower than 0.03 m/s) and only small disturbances exist mainly behind the wire electrode. It means that the time-averaged EHD secondary flow in the midplane of this non-thermal plasma reactor was in principle 2-dimensional.

The averaged flow patterns in the plane B (placed 60 mm from the side wall) in the non-thermal plasma reactor are shown in Figures 6–8. In this plane the flow velocity x- and y-component (vector map in Fig. 6) are very similar to those in the midplane (presented in Fig. 3). However, a stronger influence of the discharge on the flow patterns is visible in the velocity z-component (Fig. 8) which reaches the values up to 0.08 m/s in the discharge region and downstream.

Figures 9 and 10 show the averaged flow velocity field and corresponding flow streamlines in the plane C placed 20 mm from the side wall. As can be seen, in the upstream of the wire electrode the flow velocity field and flow streamlines are similar to those in the planes A and B. However, in the downstream of the wire electrode a pair of vortices occurs. These vortices block the flow in the centre of the non-thermal plasma reactor duct. The whole gas in the downstream region flows near the plate electrodes (velocity x-component reaches the values up to 1.3 m/s). The velocity z-component in the plane C (Fig. 11) is higher than that in the plane B and reaches the values up to 0.12 m/s.

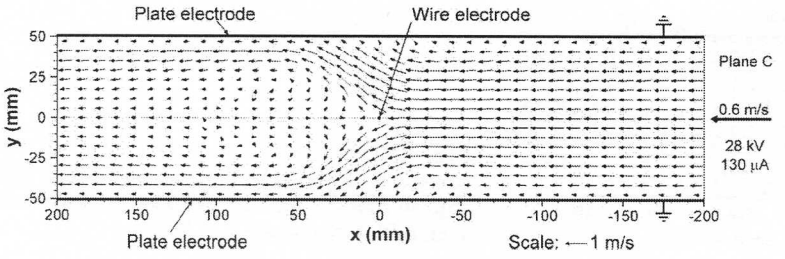

Fig. 9. Averaged flow velocity field in the plane C in the non-thermal plasma reactor. The applied voltage was 28 kV. The primary flow average velocity was 0.6 m/s.

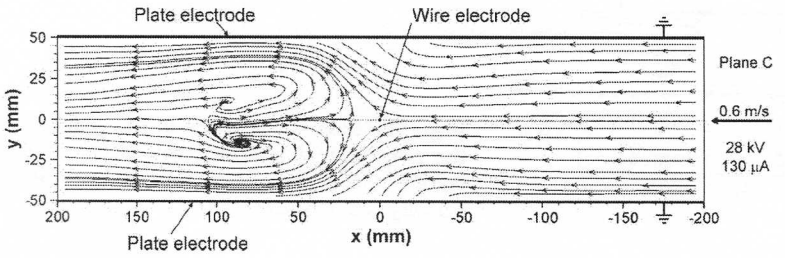

Fig. 10. Flow streamlines in the plane C in the non-thermal plasma reactor. The applied voltage was 28 kV. The primary flow average velocity was 0.6 m/s.

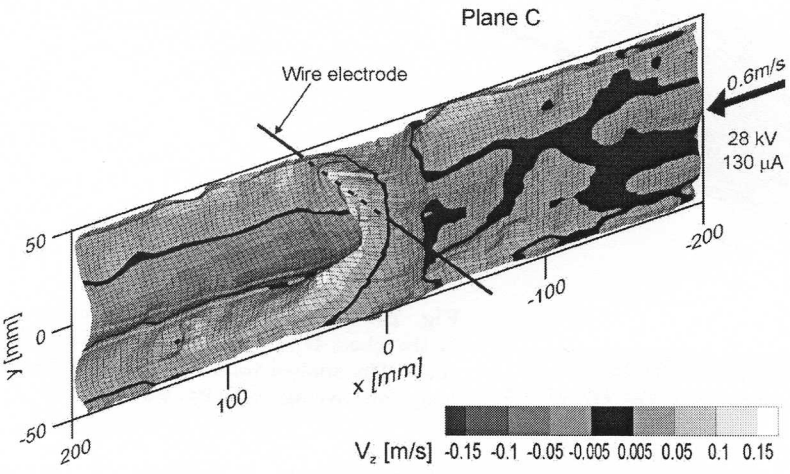

Fig. 11. Averaged flow velocity z-component in the plane C in the non-thermal plasma reactor. The applied voltage was 28 kV. The primary flow average velocity: 0.6 m/s.

The averaged flow velocity field, corresponding flow streamlines and velocity z-component measured in the plane D (placed 10 mm from the side wall) are presented in Figures 12–14, respectively. In this plane in the upstream of the wire electrode the flow velocity field and flow streamlines are again similar to those in the planes A, B and C. Similarly as in the plane C, in the downstream of the wire electrode the pair of vortices block the flow in the centre of the non-thermal plasma reactor duct and the whole gas flows near the plate electrodes. The average velocity z-component in the plane D reaches the highest values (up to 0.18 m/s).

From results presented in Figures 3–14 one can see that the flow in the upstream of the discharge region (x from −200 mm to −50 mm) is not much disturbed by the discharge in all four measured planes. In planes A and B (reactor midplane and plane placed 60 mm from the side wall) the flow is disturbed mainly in the discharge region and stabilizes in the downstream of this region. In planes C and D (placed relatively close to the side wall) the flow disturbances are much stronger than in planes A and B and are clearly visible not only in the discharge region but also in the downstream of this region.

4 Conclusions

In this paper, the results of 3D PIV measurements in the four parallel planes set along the relatively wide non-thermal plasma reactor are presented. The measured flow velocity fields illustrate complex nature of the EHD induced secondary flow in this reactor. In the three measured planes placed near the side wall the time-averaged flow velocity fields show 3D structures probably due to the boundary layer and the lack of the discharge near the acrylic wall. In the plane placed in the reactor midplane the mean flow is almost 2-dimensional in terms of time-averaged observations. However, it should be noticed that instantaneous results (not presented in this paper) exhibit

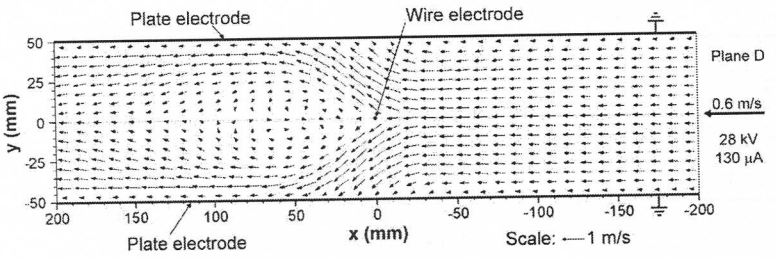

Fig. 12. Averaged flow velocity field in the plane D in the non-thermal plasma reactor. The applied voltage was 28 kV. The primary flow average velocity was 0.6 m/s.

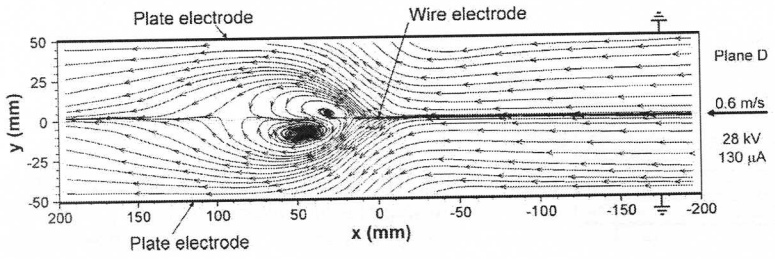

Fig. 13. Flow streamlines in the plane D in the non-thermal plasma reactor. The applied voltage was 28 kV. The primary flow average velocity was 0.6 m/s.

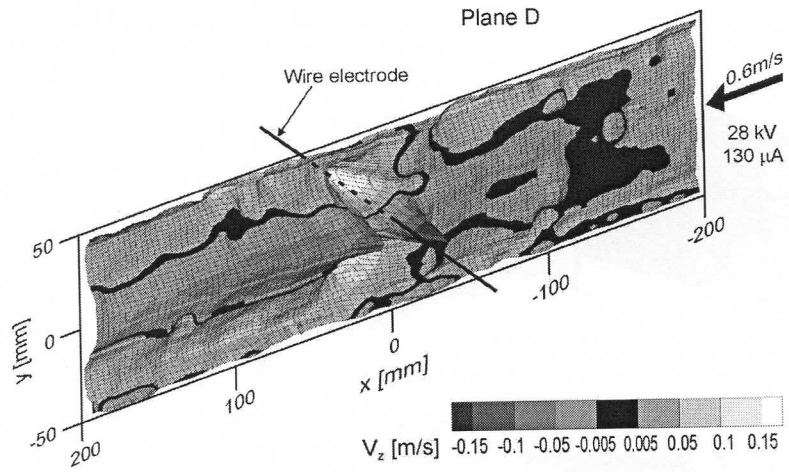

Fig. 14. Averaged flow velocity z-component in the plane D in the non-thermal plasma reactor. The applied voltage was 28 kV. The primary flow average velocity: 0.6 m/s.

that even in the reactor midplane the instantaneous EHD induced secondary flow is turbulent and 3-dimensional.

The results show clearly 3D character of the EHD secondary flow, resulting from the 3D interaction of the electric field, electric charge and the main gas flow in the non-thermal plasma rector. Even in wide non-thermal plasma reactor the EHD flow cannot be assumed to be 2-dimensional when its short-time behavior is considered.

This research has been supported by the Ministry of Science and Higher Education (grant PB 1857/B/T02/2007/33).

References

1. T. Ohkubo, S. Kanazawa, Y. Nomoto, J. Mizeraczyk, in *Proceedings of the 35th Annual Meeting – IEEE Industry Applications Society*, Roma, Italy, 2000, 1&2, pp. 864–867
2. S. Kanazawa, Y. Shuto, N. Sato, T. Ohkubo, Y. Nomoto, J. Mizeraczyk, J.S. Chang, IEEE Trans. Ind. Appl. **39**, 333 (2003)
3. J. Mizeraczyk, J. Dekowski, J. Podliński, M. Dors, M. Kocik, J. Mikielewicz, T. Ohkubo, S. Kanazawa, 3rd Triennial Special Issue "Images in Plasma Science",IEEE Trans. Plas. Sci. **30**, 164 (2002)
4. J. Mizeraczyk, J. Podliński, M. Dors, M. Kocik, S. Kanazawa, T. Ohkubo, J.S. Chang, Czech. J. Phys. D **52**, D413 (2002)
5. J. Mizeraczyk, J. Podliński, M. Dors, J. Phys. D **52**, D769 (2002)
6. J. Dekowski, J. Mizeraczyk, T. Ohkubo, S. Kanazawa, J.S. Chang, Czech. J. Phys. C **54**, 948 (2004)
7. T. Yamamoto, M. Okuda, M. Okubo, IEEE Trans. Ind. Appl. **39**, 1602 (2003)
8. Y.N. Chun, J.S. Chang, A.A. Berezin, J. Mizeraczyk, IEEE Trans. Diel. Electr. Insul. **14**, 119 (2007)
9. L. Zhao, K. Adamiak, IEEE Trans. Ind. Appl. **44**, 683 (2008)
10. M. Raffel, Ch.E. Willert, S.T. Wereley, J. Kompenhans, *Particle Image Velocimetry, A Practical Guide*, 2nd edn. (Springer-Verlag, Berlin Heidelberg, 2007)
11. P. Atten, F.M.J. McCluskey, A.C. Lahjomri, IEEE Trans. Ind. Appl. **23**, 705 (1987)
12. IEEE-DEIS-EHD Technical Committee, IEEE Trans. Diel. Electr. Insul. **10-1**, 3 (2003)